OMI measured increasing SO_2 emissions due to energy industry expansion and relocation in Northwestern China

Authors:
Zaili Ling[1], Tao Huang[1,*], Yuan Zhao[1], Jixiang Li[1], Xiaodong Zhang[1], Jinxiang Wang[1], Lulu Lian[1], Xiaoxuan Mao[1], Hong Gao[1], Jianmin Ma[2,1,3,*]

Affiliations:
[1]Key Laboratory for Environmental Pollution Prediction and Control, Gansu Province, College of Earth and Environmental Sciences, Lanzhou University, Lanzhou 730000, P. R. China
[2]Laboratory for Earth Surface Processes, College of Urban and Environmental Sciences, Peking University, Beijing, 100871, China
[3]CAS Center for Excellence in Tibetan Plateau Earth Sciences, Chinese Academy of Sciences, Beijing, 100101, China

Corresponding author: Jianmin Ma, Tao Huang
College of Earth and Environmental Sciences, Lanzhou University, 222, Tianshui South Road, Lanzhou 730000, China

Email: jianminma@lzu.edu.cn; huangt@lzu.edu.cn

Abstract

The rapid growth of economy makes China the largest energy consumer and sulfur dioxide (SO_2) emitter in the world. In this study, we estimated the trends and step changes in the planetary boundary layer (PBL) vertical column density (VCD) of SO_2 from 2005 to 2015 over China measured by the Ozone Monitoring Instrument (OMI). We show that these trends and step change years coincide with the effective date and period of the national strategy for energy development and relocation in northwestern China and the regulations in the reduction of SO_2 emissions. Under the national regulations in the SO_2 emissions reduction in eastern and southern China, SO_2 VCD in the Pearl River Delta (PRD) of southern China exhibited the largest decline during 2005-2015 at a rate of -7% yr^{-1}, followed by the North China Plain (NCP) (-6.7% yr^{-1}), Sichuan Basin (-6.3% yr^{-1}), and Yangtze River Delta (YRD) (-6% yr^{-1}), respectively. The Mann–Kendall (MK) test reveals the step change points of declining SO_2 VCD in 2009 for the PRD and 2012-2013 for eastern China responding to the implementation of SO_2 control regulation in these regions. In contrast, the MK test and regression analysis also revealed increasing trends of SO_2 VCD in northwestern China, particularly for several "hot spots" featured by growing SO_2 VCD in those large-scale energy industry bases in northwestern China. The enhanced SO_2 VCD is potentially attributable to increasing SO_2 emissions due to the development of large-scale energy industry bases in energy-abundant northwestern China under the national strategy for the energy safety of China in the 21st century. We show that these large-scale energy industry bases could overwhelm the trends and changes in provincial total SO_2

emissions in northwestern China and contributed increasingly to the national total SO_2 emission in China. Given that northwestern China is more ecologically fragile and uniquely susceptible to atmospheric pollution as compared with the rest of China, increasing SO_2 emissions in this part of China should not be overlooked and merit scientific research.

1. Introduction

Sulfur dioxide (SO_2) is one of the criteria air pollutants emitted from both anthropogenic and natural sources. The combustions of sulfur-containing fuels, such as coal and oil, are the primary anthropogenic emitters, which contributed to the half of total SO_2 emissions (Smith et al., 2011; Lu et al., 2010; Stevenson et al., 2003; Whelpdale et al., 1996). With the rapid economic growth in the past decades, China has become the world's largest energy consumer accounting for 23% of global energy consumption in 2015 (BIEE, 2016). Coal has been a dominating energy source in China and accounted for 70% of total energy consumption in 2010 (Kanada et al., 2013). The huge demand for coal and its high sulfur content make China the largest SO_2 emission source in the world (Krotkov et al., 2016; Su et al., 2011), which also accounted for two-third of Asia's total SO_2 emission (Ohara et al., 2007). From 2000 to 2006, the total SO_2 emission in China increased by 53% at an annual growth rate of 7.3% (Lu et al., 2010). To reduce SO_2 emission, from 2005 onward the Chinese government has issued and implemented a series of regulations, strategies, and SO_2 control measures, leading to a drastic decrease of SO_2 emission, particularly in eastern and southern China (Lu et al., 2011; Li et al., 2010).

Recently, two research groups led by NASA (National Aeronautics and Space Administration) and Lanzhou University of China published almost simultaneously the temporal and spatial trends of SO_2 in China from 2005 to 2015 using the OMI retrieved SO_2 PBL column density after the OMI is launched for 11 years (Krotkov et al., 2016; Shen et al., 2016). The results reported by the two groups revealed the widespread decline of SO_2 in eastern China for the past decade. Shen et al. noticed, however, that, in contrast to dramatic decreasing SO_2 emissions in densely populated and industrialized eastern and southern China, the OMI measured SO_2 in northwestern China appeared not showing a decreasing trend. This is likely resulted from the energy industry relocation and development in energy-abundant northwestern China in the past decades under the national strategy for China's energy development and safety during the 21st century. Concern is raised about the potential impact of SO_2 emissions on the ecological environment and health risk in northwestern China because high SO_2 emissions could otherwise damage the rigorous ecological environment in this part of China, featured by very low precipitation and sparse vegetation coverage which reduce considerably the atmospheric removal of air pollutants (Ma and Xu, 2017).

To assess and evaluate the risks of the ecological environment and public to the growing SO_2 emissions in northwestern China, it is necessary to investigate the spatiotemporal distributions of SO_2 concentrations and emissions. However, the ground measurements of ambient SO_2 are scarce temporally and spatially in China, and often subject to significant errors and uncertainties. Owing to the rapid progress in the remote sensing techniques, satellite retrieval of air pollutants has become a powerful tool for the assessment of emissions and spatiotemporal distributions of air pollutants. In recent several years, OMI (Dutch Space, Leiden, The Netherlands, embedded on Aura satellite) retrieved SO_2 column concentrations have been increasingly applied to elucidate the spatiotemporal variation of global and regional SO_2 levels and its emissions from large point sources, and evaluate the effectiveness of SO_2 control policies and measures (Krotkov et al., 2016; McLinden et al., 2015, 2016；Ialongo et al., 2015; Fioletov et al., 2015, 2016；Wang et al., 2015；Li et al., 2010). The decadal operation of the OMI provides the relatively long-term SO_2 time series data with a high spatial resolution which are particularly useful for assessing the changes and trends in SO_2 emissions induced by national regulations and strategies. The present study aims to (1) determine the spatiotemporal variations of SO_2 and its trend under the national plan for energy industry development in northwestern China by making use of the OMI-measured SO_2 data during 2005-2015; (2) to identify leading causes contributing to the enhanced SO_2 emission in northwestern China.

2 Data and methods

2.1 Satellite data

The OMI Ozone Monitoring Instrument (OMI) was launched on July 15, 2004, on the EOS Aura satellite, which is in a sun-synchronous ascending polar orbit with 1:45 pm local equator crossing time. It is an ultraviolet/visible (UV/VIS) nadir solar backscatter spectrometer, which provides nearly global coverage in one day, with a spatial resolution of 13 km×24 km (Levelt et al. 2006a, 2006b). It provides global measurements of ozone (O_3), SO_2, NO_2, HCHO and other pollutants on a daily basis. The OMI uses spectral measurements between 310.5 and 340 nm in the UV-2 to detect anthropogenic SO_2 pollution in the lowest part of the atmosphere (Li et al., 2013). The instrument is sensitive enough to detect the near-surface SO_2. Previously, the OMI PBL SO_2 data were produced using the Band Residual Difference (BRD) algorithm (Krotkov et al., 2006), which have large noise and unphysical biases particularly at high latitudes (Krotkov et al., 2008). Subsequently, a principal component analysis (PCA) algorithm was applied to retrieve SO_2 column densities. This approach greatly reduces biases and decreases the noise by a factor of 2, providing greater sensitivity to anthropogenic emissions (Li et al., 2013).

In the present study, we collected the level 3 OMI daily planetary boundary layer (PBL) SO_2 vertical column density (VCD) data in Dobson units (1 DU=2.69×10^{16} molecules cm^{-2}) produced by the PCA algorithm (Li et al., 2013). The spatial resolution is 0.25°×0.25° latitude/ longitude, available at Goddard Earth Sciences Data and Information Services Center (http://disc.sci.gsfc.nasa.gov/Aura/data-holdings/OMI/omso2_v003.shtml). The systematic bias of PCA retrievals is estimated as ~0.5 DU for regions between 30°S and 30°N. The bias increases to ~0.7-0.9 DU for high latitude areas with large slant column O_3 but is still a factor of two smaller than that from BRD retrievals (https://disc.gsfc.nasa.gov/Aura/data-holdings/OMI/documents/v003/omso2readme-v120-2

0140926.pdf). As a result, the PCA algorithm may yield systematic errors for anthropogenic emission sources located in different latitudes and under complex topographic and underlying surface conditions. The air mass factors (AMFs) used to convert SO_2 slant column density (SCD) into VCD are also subject to uncertainties. Fioletov et al. (2016) revealed an overall AMF uncertainty of 28% which was created by surface reflectivity, surface pressure, ozone column, and cloud fraction. As Fioletov et al. (2016) noted, the PCA retrieved SO_2 VCD was virtually derived by using an AMF of 0.36 which is best applicable in the summertime in the eastern United States (US). Wang (2014) suggested adopting AMF≈0.57 in the estimate of SO_2 VCD distribution in eastern China. In the present study, we have taken the AMFs values in China provided by Fioletov et al. (2016) to adjust OMI measured VCD in the estimation of the SO_2 emission of the main point sources in northwestern China.

2.2 SO_2 monitoring, emission, and socioeconomic data

To evaluate and verify the spatial SO_2 VCD from OMI, ground SO_2 monitoring data of 2014 through 2015 at 188 sampling sites (cities) across China (**Fig. 1**), operated by the National Environmental Monitoring Center, available at http://www.aqistudy.cn/historydata. Annually averaged SO_2 air concentrations from 2005 to 2015 in 6 capital cities in Urumqi (Xinjiang), Yinchuan (Ningxia), Beijing (BTH and NCP), Shanghai (YRD), Guangzhou (PRD), and Chongqing (Sichuan Basin) were collected from provincial environmental bulletin published by the Ministry of Environmental Protection of China (MEPC) (http://www.zhb.gov.cn/hjzl/zghjzkgb/gshjzkgb. SO_2 anthropogenic emission inventory in China with a 0.25° longitude by 0.25° latitude resolution for every two years from 2008 to 2012 was adopted from Multi resolution Emission Inventory for China (MEIC) (Li et al., 2017, available at http://www.meicmodel.org).

The socioeconomic data in China were collected from the China Statistical Yearbooks and China Energy Statistical Yearbook, published by National Bureau of Statistics of China (NBSC), (http://www.stats.gov.cn/tjsj/ndsj/;http://tongji.cnki.net/kns55/Navi/HomePage.aspx?id=N2010080088&name=YCXME&floor=1), as well as China National Environmental Protection Plan in the Eleventh Five-Years (2006-2010) and Twelfth Five-Years (2011-2015) released by MEPC (http://www.zhb.gov.cn). These data include industrial GDP, coal consumption, thermal power generation, steel production, and SO_2 emission reduction plan, and they are presented in Table 1.

2.3 Trends and step change

The long-term trends of SO_2 VCD were estimated by linear regressions of the gridded annually SO_2 VCD against their time sequence of 2005 through 2015. The gridded slopes (trends) of the linear regressions denote the increasing (positive) or decreasing (negative) rates of SO_2 VCD (Wang et al., 2016; Huang et al., 2015; Zhang et al., 2015, 2016).

The Mann-Kendall (MK) test was also employed in the assessments of the temporal trend and step change point year of SO_2 VCD time series. The MK test is a nonparametric statistical test (Mann,1945; Kendall, 1975), which is useful for assessing the significance of trends in time series data (Waked et al., 2016; Fathian et al., 2016). The MK test is often used to detect a step change point in the long term trend of a time series dataset (Moraes et al., 1998; Li et al., 2016; Zhao et al., 2015). It is suitable for non-normally distributed data and censored data which are not influenced by abnormal values (Yue and Pilon, 2004; Sharma et al. 2016; Yue and Wang., 2004; Gao et al. 2016; Zhao et al., 2015). Recently, MK-test has also been used in trend analysis for the time series of atmospheric chemicals, such as persistent organic pollutants, surface ozone (O_3), and non-methane hydrocarbon (Zhao et al., 2015; Assareh et al.,2016; Waked et al.,2016; Sicard et al., 2016). Here the MK test was used to identify the temporal variability and step change point of SO_2 VCD for 2005-2015 which may be associated with the implementation of the national strategy and regulation in energy industry development and emission control during this period. Under the null hypothesis (no trend), the test statistic was determined using the following formula:

$$S_k = \sum_{i=1}^{k} r_i \ (k= 2, 3, ...,n) \tag{1}$$

where S_k is a statistic of the MK test, and

$$r_i = \begin{cases} +1, (x_i > x_j) \\ 0, (x_i \leq x_j) \end{cases} \quad (j=1,2, ...,i\text{-}1) \tag{2}$$

where x_i is the variable in time series x_1, x_2, ..., x_i, r_i is the cumulative number for x_i>x_j. The test statistic is normally distributed with a mean and variance is given by:

$$E(S_k) = k(k-1)/4 \tag{3}$$

$$Var(S_k) = \frac{k(k-1)(2k+5)}{72} \tag{4}$$

From these two equations, one can derive a normalized S_i, defined by

$$UF_k = \frac{S_k - E(S_k)}{\sqrt{Var(S_k)}} \quad (k=1, 2, ...,n) \qquad (5)$$

where UF_k is the forward sequence, the backward sequence UB_k is calculated using the same function but with the reverse data series such that UB_k=-UF_k.

In a two-sided trend test, a null hypothesis is accepted at the significance level if $|(UF_k)| \le (UF_k)_{1-\alpha/2}$, where $(UF_k)_{1-\alpha/2}$ is the critical value of the standard normal distribution, with a probability of a. When the null hypothesis is rejected (i.e., when any of the points in UF_k exceeds the confidence interval ±1.96; P=0.05), a significantly increasing or decreasing trend is determined. UF_k> 0 often indicates an increasing trend and vice versa. The test statistic used in the present study enables us to discriminate the approximate time of trend and step change by locating the intersection of the UF_k and UB_k curves. The intersection occurring within the confidence interval (-1.96, 1.96) indicates the beginning of a step change point (Moraes et al., 1998; Zhang et al., 2011; Zhao et al., 2015).

2.4 Estimate of SO_2 emission from OMI measurements

To assess the connections between the major point sources in large-scale energy industrial bases in northwestern China and provincial emissions, we made use of OMI measured SO_2 VCD to inversely simulate the SO_2 emission from Ningdong Energy Chemical Industrial Base (NECIB) in Ningxia and Midong Energy Industrial Base (MEIB) in Xinjiang. McLinden et al. (2016) and Fioletov et al. (2015, 2016) have developed a source detection algorithm which fits OMI-measured SO_2 vertical column densities to a three-dimensional parameterization function of the horizontal coordinates and wind speed. This algorithm was employed in the present study to estimate the SO_2 source strength in the two industrial bases and its contribution to the provincial total SO_2 emissions. The details of this algorithm are referred to Fioletov et al (2015). Briefly, the source detection algorithm uses a Gaussian function $f(x, y)$ multiplied by an exponentially modified Gaussian function $g(y, s)$ to fit the OMI SO_2 measurements (Fioletov et al., 2015) $OMI_{SO_2} = a \cdot f(x,y) \cdot g(y,s)$, defined by

$$
\begin{aligned}
&f(x,y) = \frac{1}{\sigma_1\sqrt{2\pi}}\exp(-\frac{x^2}{2\sigma_1^{\ 2}});\\
&g(y,s) = \frac{\lambda_1}{2}\exp(\frac{\lambda_1(\lambda_1\sigma^2+2y)}{2})\cdot \text{erfc}(\frac{\lambda_1\sigma^2+y}{\sqrt{2}\sigma});\\
&\sigma_1 = \begin{cases}\sqrt{\sigma^2-1.5y}, y<0\\ \sigma, y\geq 0\end{cases};\\
&\lambda_1 = \lambda / s;\\
&\text{erfc}(x) = \frac{2}{\sqrt{\pi}}\int_x^{\infty} e^{-t^2}\,dt
\end{aligned}
\qquad (6)
$$

where x and y indicate the coordinates of the OMI pixel center (km); s is the wind speed (km h^{-1}) at the pixel center; a represents the total number of SO_2 molecules (or SO_2 burden) observed by OMI in a target emission source $\lambda = 1/\tau$, where τ is a decay time of SO_2, and σ describes the width or spread of SO_2.

The $f(x, y)$ function represents the Gaussian distribution across the wind direction line. The function $g(y, s)$ represents an exponential decay along the y-axis smoothed by a Gaussian function. Once σ and τ are determined, the SO_2 burden as a function of x, y, and s (OMI SO_2 (x, y, s)) can be reconstructed. SO_2 emission strength from a large point source can be estimated by $E=a/\tau$. In the present study, following Fioletov

(2016) we choose a mean value of σ=20 km and *τ*=6 h in the calculation of SO_2 emission large point sources of interested. Wind speed and direction on a 1°×1° latitude/longitude spatial resolution were collected from NCEP (National Centers for Environmental Prediction) Final Operational Global Analysis (http://dss.ucar.edu/datasets/ds083.2/). These data were interpolated to the location of each OMI pixel center on a 1/4°×1/4° latitude/longitude spacing.

There are several potential sources of errors which need to be taken into account when determining the overall uncertainty of the SO_2 emission estimation. Fioletov et al. (2016) have highlighted three primary sources of errors in the OMI-based emission estimates, including AMF, the estimation of the total SO_2 mass as determined from a linear regression, and the selection of σ and *τ* used to fit OMI measurements. Based on the coefficients of variation (*CV,* %) in these three error categories (McLinden et al., 2014, 2016; Fioletov et al.; 2016) listed in **Table S1** of Supplement, we estimated uncertainties in the SO_2 emissions derived from OMI measurements in the two major point sources in northwestern China by running the source detection model repeatedly for 10,000 times using Monte Carlo method. Results show the standard deviation of -35 to 122 kt/yr for SO_2 emissions in NECIB and -29 to 95 kt/yr for SO_2 emissions in MEIB from 2005 to 2015, respectively.

2.5 Satellite data validation

The OMI retrieved SO_2 PBL VCDs were evaluated by comparing with ambient air concentration data of SO_2 from routine measurements by local official operational air quality monitoring stations. The statistics between OMI retrieved SO_2

VCD and monitored annually averaged SO_2 air concentrations during 2014-2015 at 188 operational air quality monitoring stations across China are presented in **Table S2** of Supplement. **Figure S1** is the correlation diagram between SO_2 VCD and sampled data. As shown in **Table S2** and **Fig. S1**, the OMI measured SO_2 VCDs agree well with the monitored ambient SO_2 concentrations across China at the correlation coefficient of 0.85 ($p<0.05$) (**Table S2**). **Figure 2** further compares annually averaged SO_2 VCD and SO_2 air concentrations from 2005 to 2015 in 6 capital cities. These are Urumqi, Yinchuan, Beijing, Shanghai, Guangzhou, and Chongqing, respectively. The mean SO_2 concentration data were collected from provincial environmental bulletin published by the Ministry of Environmental Protection of China (MEPC) (http://www.zhb.gov.cn/hjzl/zghjzkgb/gshjzkgb). Results show that the annual variation of mean SO_2 VCD are higher than the measured SO_2 concentrations from 2010 to 2015, but SO_2 VCD match well with the monitored data except for Urumqi, the capital of Xinjiang Uygur Autonomous Region. The OMI retrieved SO_2 VCDs in Shanghai and Chongqing are higher than the measured concentrations in these two regions show consistent temporal fluctuation and trend. The measured SO_2 concentrations peaked in 2013 in Yinchuan whereas the SO_2 VCD reached the peak in 2012 and decreased thereafter. OMI measured SO_2 VCD in Urumqi shows different yearly fluctuations compared with its annual concentrations. The measured SO_2 concentrations in Urumqi decreased from 2011 to 2015 whereas the OMI measured SO_2 VCD did not illustrate obvious changes. In particular, the monitored mean SO_2 concentration from 2013 to 2015 decreased by 75% compared with that from 2005 to 2012. This is partly attributed to the change in air quality monitoring sites in Urumqi city. Before 2013, there were only three operational air quality sites in Urumqi City, all located in the heavily polluted downtown region. Since 2013, the air monitoring sites increased from 3 to 7. The four new sites are located in less polluted suburbs of the city. As a result, the spatially averaged SO_2 concentrations over 3 downtown air quality monitoring sites before 2013 were higher than the mean concentrations averaged over 7 monitoring sites (http://xjny.ts.cn/content/2012-06/05/content_6899388.htm). It is worth noting that the measured SO_2 concentration in Urumqi is the highest among all cities as shown in Fig. 2 whereas the OMI VCD value in Urumqi was lower than other selected cities. This may be due to systematic biases in OMI-retrieved SO_2 VCD. In the present study, the level 3 OMI PBL SO_2 VCD data produced by the PCA retrievals were used to estimate the spatiotemporal variation in SO_2 pollution in China. The PCA retrievals have a negative bias over some highly reflective surfaces in arid and semi-arid lands, such as many some places in the Sahara (up to about -0.5 DU in monthly mean VCD) (https://disc.gsfc.nasa.gov/Aura/data-holdings/OMI/documents/v003/omso2readme-v120-20140926.pdf). Also, PCA retrievals is subject to the systematic bias of 0.7-0.9 DU in relatively high latitude regions. Located at a relatively high latitude in northwestern China with a large surrounding area covered by Gobi desert, the PCA algorithm might yield lower SO_2 VCD value in Urumqi than other cities shown in **Fig. 2**.

SO_2 emissions data were further collected to compare with annual OMI SO_2 VCD in selected regions. The results are presented in **Fig. 3**. As shown, the annual variation in SO_2 VCD agrees reasonably well with SO_2 emission data except for Urumqi-Midong region. The OMI measured SO_2 VCD in the PRD and Sichuan Basin decreased from 2008 to 2012, but SO_2 emission changed little. Compared with the other five marked regions (**Fig. 1**), the satellite measured SO_2 VCD in Urumqi-Midong declined in 2010 and inclined in 2012. However, SO_2 emissions in Urumqi-Midong 2012 are factors of 11 and 8 higher than that in 2008 and 2010, respectively. It should be noted that air pollutants released in the atmosphere are affected by physical and chemical processes. They may be transported over large distances by atmospheric motions, transformed into other compounds by chemical or photochemical processes, and "washed out" or deposited at the Earth's surface (Zhao et al., 2017; Brasseur et al., 1998). The atmospheric removal and advection processes may also contribute to the inconsistency between monitored and satellite observations. In addition, the MEIC SO_2 emission inventory from the bottom-up approach might be subject to large uncertainties due to data manipulation, and the lack of sufficient knowledge in human activities and emissions from different sources (Li et al., 2017; Zhao et al., 2011; Lu et al., 2011; Kurokawa et al., 2013). The uncertainties in the MEIC estimated SO_2 emissions used in the present study are up to ±12% (Li et al., 2017). As shown in **Fig. 3**, the OMI measured SO_2 VCD from 2008 to 2012 in Urumqi-Midong was about 0.2 DU which was comparable with that in the EGT. However, the reported SO_2 emission in Urumqi-Midong was only 4% of the SO_2

emission in the EGT in 2012 and 0.5% of that in the EGT from 2008 to 2010. It might be subject to that part large SO_2 emission sources were not included in emission inventory. From this perspective, the satellite remote sensing provides a very useful tool in monitoring SO_2 emissions from large point sources and in the verification of emission inventories (Fioletov et al., 2015, 2016; McLinden et al., 2016; Wang et al., 2015;).

3 Results and discussion

3.1. OMI measured SO_2 in China

Given higher population density and stronger industrial activities, eastern and southern China are traditionally industrialized and heavily contaminated regions by air pollutions and acid rains caused by SO_2 emissions. **Figure 4a** shows annually averaged OMI SO_2 VCD over China on a 0.25° × 0.25° latitude/longitude resolution averaged from 2005 to 2015. SO_2 VCD was higher considerably in eastern and central China, and Sichuan Basin than that in northwestern China. The highest SO_2 VCD was found in the NCP, including Beijing-Tianjin-Hebei (BTH), Shandong, and Henan province. The annually averaged SO_2 VCD between 2005-2015 in this region reached 1.36 DU. This result is in line with previous satellite remote sensing retrieved SO_2 emissions in eastern China (Krotkov et al 2016; Lu et al., 2010; Bauduin et al., 2016; Jiang et al 2012; Yan et al., 2014). However, in contrast to the spatial distribution of decadal mean SO_2 VCD (**Fig. 4a**), the slopes of the linear regression relationship between annual average OMI-retrieved SO_2 VCD and the time sequence from 2005 to 2015 over China show that the negative trends overwhelmed industrialized eastern and southern China, particularly in the NCP, Sichuan Basin, the YRD, and PRD, manifesting significant decline of SO_2 emissions in these regions. SO_2 VCD in the PRD exhibited the largest decline at a rate of 7% yr^{-1}, followed by the NCP (6.7% yr^{-1}), Sichuan Basin (6.3% yr^{-1}), and the YRD (6% yr^{-1}), respectively. Annual average SO_2 VCD in the PRD, NCP, Sichuan Basin, and YRD decreased by 52%, 50% , 48%, and 46% in 2015 compared to 2005 (**Fig. 5**), though the annual fluctuation of SO_2 VCD shows rebounds in 2007 and 2011 which are potentially associated with the economic resurgence stimulated by the central government of China (He et al., 2009; Diao et al., 2012). The reduction of SO_2 VCD after 2011 in these regions reflects virtually the response of SO_2 emissions to the regulations in the reduction of SO_2 release, the mandatory application of the flue-gas desulfurization (FGD) on coal-fired power plants and heavy industries, and the slowdown in the growth rate of the Chinese economy (CSC, 2011a; Wang et al., 2015, Chen et al., 2016).

Since in the MK test the signs and fluctuations of UF_k are often used to predict the trend of a time series, this approach is further applied to quantify the trends and step changes in annually SO_2 VCD time series in those highlighted regions (a-f) in **Fig. 4b** from 2005 to 2015. Results are illustrated in **Fig. 6**. As shown, the forward and backward sequences UF_k and UB_k intersect at least once from 2005 to 2015. These intersections are all well within the confidence levels between -1.96 and 1.96 at the statistical significance α=0.01. A common feature of the forward sequence UF_k in eastern and southern China provinces is that UF_k has been declining and become negative from 2007 to 2009 onward (**Fig. 6a-d)**, confirming the downturn of SO_2 atmospheric emissions and levels in these industrialized and well-developed regions in China. The step change points of OMI measured SO_2 VCDs in the NCP, YRD and Sichuan Basin occurred between 2012 and 2013. These step change points coincide with the implementation of the new Ambient Air Quality Standard in 2012, which set a lower ambient SO_2 concentration limit in the air (MEPC, 2012), and the Air Pollution Prevention and Control Action Plan in 2013 by the State Council of China (CSC, 2013a). This Action Plan requests to take immediate actions to control and reduce air pollution in China, including cutting down industrial and mobile emission sources, adjusting industrial and energy structures, and promoting the application of clean energy in the BTH, YRD, PRD and Sichuan Basin. The step change in SO_2 VCD over the PRD occurred in the earlier year of 2009-2010 and from this period onward the decline of SO_2 VCD speeded up, as shown by the forward sequence UF_k which became negative since 2007 and was below the confidence level of -1.96 after 2009, suggesting significant decreasing VCD from 2009 (**Fig. 6c)**. In April 2002, the Hong Kong Special Administrative Region (HKSAR) Government and the Guangdong Provincial Government reached a consensus to reduce, on a best endeavor basis, the anthropogenic emissions of SO_2 by 40% in the PRD by 2010, using 1997 as the base year (http://www.epd.gov.hk/epd/english/action_blue_sky/files/exsummary_e.pdf). By the end of 2010, all thermal power units producing more than 0.125 million kilowatts electricity in the PRD were equipped with the FGD. During the 11th Five-Year Plan (2006-2010), the thermal power units with 1.2 million kilowatts capacity have been shut down. SO_2 emission was reduced by 18% in 2010 compared to that in 2005 (NBSC, 2006, 2011). This likely caused the occurrence of the step change in SO_2 VCD over 2009-2010.

3.2. OMI measured SO_2 "hot spots" in northwestern China

As also shown in **Fig. 4b**, in contrast to widespread decline of SO_2 VCD, there are two "hot spots" featured by moderate increasing trends of SO_2 VCD, located in the China's Energy Golden Triangle (EGT, Shen et al., 2016, Ma and Xu, 2017) and Urumqi-Midong region in northwestern China. The annual growth rate of SO_2 VCD from 2005 to 2015 are 3.4% yr^{-1} in the EGT and 1.8% yr^{-1} in Urumqi-Midong, respectively (**Fig. 4b**). SO_2 VCD in these two regions peaked in 2011 and 2013 which were 1.6 and 1.7 times of that in 2005 (**Fig. 5**). The raising SO_2 VCD in the part of the EGT have been reported by Shen et al. (2016). The second hot spot is located in Urumqi-Midong region including MEIB that is about 40 km away from Urumqi. The both EGT and MEIB are featured by extensive coal mining, thermal power generation, coal chemical, and coal liquefaction industries. The reserve of coal, oil and natural gas in the EGT is approximately 1.05×10^{12} ton of standard coal equivalent, accounting for 24% of the national total energy reserve in China (CRGECR, 2015). It has been estimated that there are deposits of 20.86 billion tons of oil, 1.03 billion cubic meters of natural gas, and 2.19 trillion tons of coal in Xinjiang, accounting for 30%, 34% and 40% of the national total (Dou, 2009). Over the past decades, a large number of energy-related industries have been constructed in northwestern China, such as the EGT and MEIB to enhance China's energy security in the 21st century and speed up the local economy. The rapid development of energy and coal chemical industries in Ningxia Hui Autonomous Region and Xinjiang of northwestern China alone resulted in the significant demands to coal mining and coal products. The coal consumption, thermal power generation, and the gross industrial output increased by 2.7, 3.5, and 6.6 times in Ningxia from 2005 to 2015, and by 2.7, 4.2 and 6.6 times in Xinjiang during the same period (NBSC, 2005, 2015). As a result, SO_2 emissions increased markedly in these regions, as shown by the increasing trends of SO_2 VCD in the EGT and Urumqi-Midong region (**Fig. 4b**).

The MK forward sequence further confirms the increasing SO_2 VCD in the EGT and Urumqi-Midong. As seen in **Fig. 6e** and **6f**, the UF_k values for SO_2 VCD are positive and growing, illustrating clear upward trends of SO_2 VCD over these two large-scale energy industry bases, revealing the response of SO_2 emissions to the energy industry relocation and development in northwestern China. To guarantee the national energy security and to promote the regional economy, the EGT energy program has been accelerating since 2003 under the national energy development and relocation plan (Zhu and Ruth, 2015; Chen et al., 2016), characterized by the rapid expansion of the NECIB which is located about 40 km away from Yinchuan, the capital of Ningxia (Shen et al., 2016). By the end of 2010, a large number of coal chemical industries, including the world largest coal liquefaction and thermal power plants, have been built and operated, and the total installed capacity of thermal power generating units has reached 1.47 million kilowatts (Zhao, 2016). Under the same national plan, the MEIB in Xinjiang started to construction and operation from the early to mid-2000s which have almost the same industrial structures as those in the EGT, featured by coal-fired power generation, coal chemical industry, and coal liquefaction.

The statistical significant step change points of SO_2 VCD in the EGT and Urumqi-Midong took place in 2006 and 2009 (**Fig. 6e** and **6f**), differing from those regions with decreasing trends of SO_2 VCD in eastern and southern China. The first step change point in 2006-2007 corresponds to the increasing SO_2 emissions in these two large-scale energy bases till their respective peak emissions in EGT (2007) and Urumqi-Midong (2008). The second step change point in 2009 coincides with the global financial crisis in 2008 which slowed down considerably the economic growth in 2009 in China, leading to raw material surplus and the remarkable reduction in the demand for coal products.

3.3 OMI SO_2 time series and step change point year in northwestern China

The clearly visible "hot spots" featured by increasing OMI measured SO_2 VCD in the EGT/NECIB and MEIB raise a question: to what extent could these large-scale energy industrial bases affect the trend and fluctuations of SO_2 emissions in northwestern China？**Figure 7** illustrates the fractions (%) of OMI measured annual SO_2 VCD and SO_2 emissions averaged over the 6 provinces of northwestern China in the annual national total VCD (**Fig. 7a**) and emissions (**Fig. 7b**) from 2005 to 2015. The both SO_2 VCD and emission fractions in northwestern China in the national total increased over the past decade. By 2015, the mean SO_2 VCD fraction in 6 northwestern provinces has reached 38% in the national total. The mean emission fraction was about 20% in the national total. It should be noted that there were large uncertainties in provincial SO_2 emission data which often underestimated SO_2 emissions from major point sources (Li et al., 2017; Han et al., 2007). In this sense, OMI retrieved SO_2 VCD fraction provides a more reliable estimate to the contribution of SO_2 emission in northwestern China to the national total.

The annual percentage changes in SO_2 VCD from 2005 onward are consistent well with the per capita SO_2 emissions in China (**Fig. 8**). As aforementioned, while the annual total SO_2 emissions in the well-developed BTH, YRD, and PRD were higher than that in northwestern provinces, the per capita emissions in all provinces of northwestern China, especially in Ningxia and Xinjiang where the NECIB and MEIB are located, were about factors of 1 to 6 higher than that in the BTH, YRD, and PRD, as shown in **Fig. 8**. In contrast to declining annual emissions from the BTH, YRD, and PRD, the per capita SO_2 emissions in almost all western provinces have been growing from 2005 onward.

Since almost all large-scale coal chemical, thermal power generation, and coal liquefaction industries were built in energy-abundant and sparsely populated northwestern China over the past two decades, particularly since the early 2000s, those large-scale industrial bases in this part of China likely play an important role in the growing SO_2 emissions in northwestern provinces. We further examine the OMI retrieved SO_2 VCD to confirm and evaluate the changes in SO_2 emissions in northwestern China which should otherwise respond to these large-scale energy programs under the national plan for energy relocation and expansion. **Figure 9** displays the MK test statistics for SO_2 VCD in the 6 provinces in northwestern China from 2005-2015. The forward sequence UF_k suggests decreasing trends in Shaanxi and Gansu provinces and a moderate increase in Qinghai province. In Xinjiang and Ningxia where the most energy industries were relocated and developed for the last decade (2005-2015), as aforementioned, UF_k time series estimated using SO_2 VCD data illustrate clear upward trends. Compared with those well-developed regions in eastern and southern China, the UF_k values of SO_2 VCD in these northwestern provinces are almost all positive, except for Shaanxi province where the UF_k turned to negative from 2008， and Gansu province where the UF_k value become negative during 2012-2013.

The step change points identified by the MK test for SO_2 VCD in northwestern China appear associated strongly with the development and use of coal energy. As shown in **Fig. 9**, the intersection of the forward and backward sequences UF_k and UB_k within the confidence levels of -1.96 (straight green line) to 1.96 (straight purple line) can be identified in 2006 and 2007 in Ningxia and Xinjiang, respectively, corresponding well to the expansion of two largest energy industry bases from 2003 onward in Ningxia (NECIB) and Xinjiang (MEIB). The step change point of SO_2 VCD in 2012 in Gansu province coincides with fuel-switching from coal to gas in the capital city (Lanzhou) and many other places of the province initiated from 2012 (CSC, 2013b). The MK derived step change point in Shaanxi province occurred in

2010 which was a clear signal of marked decline of fossil fuel products in northern Shaanxi where, as the part of the EGT (Ma and Xu, 2017) of China, the largest energy industry base in the province is located, right after the global financial crisis.

It is interesting to note that the forward sequences UF_k of SO_2 VCD (**Fig. 9e** and **f)** in Ningxia and Xinjiang exhibit the similar fluctuations as that in Ningdong (NECIB) and Urumqi-Midong (MEIB) (**Fig. 9e** and **f**), manifesting the potential associations between the SO_2 emissions in these two large-scale energy industrial bases (major point sources) and provincial emissions in Ningxia and Xinjiang, respectively. This suggests that large-scale energy industrial bases might likely overwhelm or play an important role in the SO_2 emissions in those energy-abundant provinces in northwestern China. **Figure 10** illustrates mean SO_2 VCD from 2005 to 2015 in northern Xinjiang (**Fig. 10a**) and Ningxia (**Fig. 10b**). The largest concentrations can be seen clearly in the MEIB and the NECIB in these two minority autonomous regions of China. Lower SO_2 concentrations are illustrated in mountainous areas of northern Xinjiang. Based on inverse modeling of SO_2 burdens (a, 10^{26} molecules) in the source detection model (section 2.4), we estimated SO_2 emission (E, kt yr^{-1}) in the NECIB and MEIB from 2005 to 2015, defined by $E=a/\tau$, where τ is a decay time of SO_2 (section 2.4). The results are illustrated in **Fig. 11.** As shown, the SO_2 emission increased from 2005 and reached the maximum in 2011 in the NECIB and declined thereafter, in line with the annual SO_2 VCD fluctuations in this energy industry base which is, as aforementioned, attributable to the economic rebound in 2011 in China. Of particular interest is the large fractions of the estimated

SO_2 emission in the NECIB in Ningxia Province (**Fig. 11a**) from 2005 to 2015. These large fractions suggest that this energy industry park alone contributed up to more than 50% emission to the provincial total SO_2 emission. Likewise, the OMI SO_2 VCD derived SO_2 emissions in the MEIB also made an appreciable contribution (15-20%) to the provincial total SO_2 emission in Xinjiang. Covered by a large area of Gobi desert (Junngar Basin), there are only a few of SO_2 emission sources in vast northern Xinjiang region (total area of Xinjiang is 1.66×10^6 km^2). This likely leads to the small fractions of SO_2 emissions in the MEIB in the total SO_2 emission in Xinjiang. **Figure 11c** and **11d** show SO_2 VCDs (the left y-axis) and the ratios (the right y-axis) of the mean VCDs in NECIB and MEIB to the provincial mean VCDs in Ningxia and Xinjiang from 2005 to 2015, respectively. It can be seen that the maximum mean SO_2 VCD over the MEIB is about a factor of 4.5 greater than the mean SO_2 VCD over Xinjiang province (**Fig. 11d**), This ratio is larger than the ratio (2.9) of the SO_2 VCD in the NECIB to the SO_2 VCD averaged over Ningxia province (**Fig. 11c**). Nevertheless, overall our results manifest that, although there were only a small number of SO_2 point sources in these two energy industrial bases, the SO_2 emissions from the NECIB and MEIB made significant contributions to provincial total emissions. Given that the national strategy for China's energy expansion and safety during the 21st century is, to a large extent, to develop large-scale energy industry bases in northwestern China, particularly in Xinjiang and Ningxia (Zhu and Ruth, 2015; Chen et al., 2016) where the energy resources are most abundant in China, we would expect that the rising SO_2 emissions in northwestern China would increasingly be attributed to those large-scale energy industry bases and contributed to the national total SO_2 emission in China.

Table 1 presents the annual average growth rates of SO_2 VCD, industrial (second) Gross Domestic Product (GDP), and major coal-consuming industries in northwestern China and three developed areas (BTH, YRD, PRD) in eastern and southern China. The positive growth rates of SO_2 VCD can be observed in the three provinces and autonomous regions (Qinghai, Ningxia, and Xinjiang) of northwestern China. Although the growth rates of SO_2 VCD in other two provinces (Gansu and Shaanxi) are negative, the magnitudes of the negative growth rates are smaller than those in the BTH, YRD, and PRD, except for Zhejiang province in the YRD. This regional contrast reflects both their economic and energy development activities and the SO_2 emission control measures implemented by the local and central governments of China. Although China has set a national target of 10% SO_2 emission reduction (relative to 2005) during 2006-2010 and 8% (relative to 2010) during 2011-2015 (CSC, 2007; CSC, 2011b), under the Grand Western Development Program of China， the regulation for SO_2 emission control was waived in those energy-abundant provinces of northwestern China in order to speed up the large-scale energy industrial bases and local economic development, and improve local personal income. Also, although FGDs were widely installed in coal-fired power plants and other industrial sectors since the 1990s, by 2010 as much as 57% of these systems were installed in eastern and southern China (Zhao et al., 2013). The capacity of small power generators which were shut-down in western China was merely about 10808 MW, only accounting for about 19% of the capacity of total small power plants which were eliminated in China (55630 MW) during the 11th Five-Year Plan period (2006-2010) (Cui et al., 2016). As shown in **Table 1**, the SO_2 emission reduction plans virtually specified the zero percentage of SO_2 emission reductions in Qinghai, Gansu, and Xinjiang and lower reduction percentage in the emission reduction in Ningxia and Inner Mongolia as compared to eastern and southern China during the 11th (2006-2010) and 12th (2011-2015) Five-Year Plan. As a result, the average growth rate for thermal power generation, steel production, and coal consumption from 2005 to 2015 in northwestern China reached 14.1% yr^{-1}, 35.7% yr^{-1}, and 11.9% yr^{-1}, considerably higher than the averaged growth rates over eastern and southern China (5.9% yr^{-1} in the BTH, 0.8% yr^{-1} in the YRD, and 2.3% yr^{-1} in the PRD).

4 Conclusions

The spatiotemporal variation in SO_2 concentration during 2005-2015 over China was investigated by making use of the PBL SO_2 column concentrations measured by the OMI. The highest SO_2 VCD was found in the NCP, the most heavily polluted area by SO_2 in China, including Beijing-Tianjin-Hebei, Shandong, and Henan province. Under the national regulation for SO_2 control and emission reduction, the SO_2 VCD in eastern and southern China underwent widespread decline during this period. However, the OMI measured SO_2 VCD detected two "hot spots" in the EGT (Ningxia-Shaanxi-Inner Mongolia) and Midong (Xinjiang) energy industrial bases, in contrast to the declining SO_2 emissions in eastern and southern

China, displaying an increasing trend with the annual growth rate of 3.4% yr^{-1} in the EGT and 1.8% yr^{-1} in Midong, respectively. The trend analysis further revealed enhanced SO_2 emissions in most provinces of northwestern China likely due to the national strategy for energy industry expansion and relocation in energy-abundant northwestern China. As a result, per capita SO_2 emission in northwestern China has exceeded industrialized and populated eastern and southern China, making increasing contributions to the national total SO_2 emission. The estimated SO_2 emissions in the Ningdong (Ningxia) and Midong (Xinjiang) energy industrial bases from OMI measured SO_2 VCD showed that the SO_2 emissions in these two industrial bases made significant contributions to the total provincial emissions. This indicates, on one side, that the growing SO_2 emissions in northwestern China would increasingly come from those large scale energy industrial bases under the national energy development and relocation plan. On the other side, this fact also suggests that it is likely more straightforward to control and reduce SO_2 emissions in northwestern China because the SO_2 control measures could be readily implemented and authorized in those state-owned large-scale energy industrial bases.

The Supplement related to this article is available online

Acknowledgements. This work is supported by the National Natural Science Foundation of China (grants 41503089, 41371478, and 41671460), Gansu Province Science and Technology Program for Livelihood of the People (1503FCMA003), the Natural Science Foundation of Gansu Province of China (1506RJZA212), and

Fundamental Research Funds for the Central Universities (lzujbky-2016-249 and lzujbky-2016-253). We thank Dr. Vitali Fioletov for his suggestions and advice during the preparation of this manuscript.

Reference

Assareh, N., Prabamroong, T., Manomaiphiboon, K., Theramongkol, P., Leungsakul, S., Mitrjit, N., and Rachiwong, J.: Analysis of observed surface ozone in the dry season over Eastern Thailand during 1997–2012, Atmos. Res., 178, 17-30, doi: 10.1016/j.atmosres.2016.03.009, 2016.

Bauduin, S., Clarisse, L., Hadji-Lazaro, J., Theys, N., Clerbaux, C., and Coheur, P. F.: Retrieval of near-surface sulfur dioxide (SO_2) concentrations at a global scale using IASI satellite observations, Atmos. Meas. Tech., 9, 721-740, doi: 10.5194/amt-9-721-2016, 2016.

BIEE (British Institute of Energy Economics): BP Statistical Review of World Energy June 2016, Available at: http://www.bp.com/content/dam/bp/pdf/energy-economics/statistical-review-2016/bp-statistical-review-of-world-energy-2016-full-report.pdf (last access: 21 January 2017), 2016.

Brasseur, G. P., Hauglustaine, D. A., Walters, S., Rasch, P. J., Müller, J. F., Granier, C., and Tie, X. X.: MOZART, a global chemical transport model for ozone and related chemical tracers: 1. Model description, J Geophys. Res., 103, 28265−28289, doi: 10.1029/98JD02397, 1998.

Chen, J., Cheng, S., Song, M., and Wang, J.: Interregional differences of coal carbon dioxide emissions in China, Energ. Policy, 96, 1−13, doi: 10.1016/j.enpol.2016.05.015, 2016.

CRGECR (The Comprehensive Research Group for Energy Consulting and Research): Strategy on the Development of Energy "Golden Triangle", Engineering Science., 9, 18-28, 2015 (in Chinese).

CSC (China's State Council): China National Environmental Protection Plan in the 11th Five-year (2006-2010), Available at: http://www.gov.cn/zwgk/2007-11/26/content_815498.htm (last access: 21 January 2017), 2007 (in Chinese).

CSC (China's State Council): Circular on accelerating the number of comments on shutting down small thermal power units in China, Available at http://www.gov.cn/zwgk/2007-01/26/content_509911.htm (last access: 21 January 2017), 2011a (in Chinese).

CSC (China's State Council): China National Environmental Protection Plan in the 12th Five-year (2011-2015), Available at: http://www.gov.cn/zwgk/2011-12/20/content_2024895.htm (last access: 21 January 2017), 2011b (in Chinese).

CSC (China's State Council): Air Pollution Prevention and Control Action Plan, Available at: http://www.gov.cn/zhengce/content/2013-09/13/content_4561.htm (last access: 21 January 2017), 2013a (in Chinese).

CSC (China's State Council): Determination, Measures and Strength-Lanzhou pollution control reproduce the blue sky, Available at: http://www.gov.cn/jrzg/2013-02/03/content_2325835.htm (last access: 21 January 2017), 2013b (in Chinese).

Cui, Y., Lin, J., Song, C., Liu, M., Yan, Y., Xu, Y., and Huang, B.: Rapid growth in nitrogen dioxide pollution over Western China, 2005-2013. Atmos. Chem. Phys., 16, 6207-6221, doi: 10.5194/acp-16-6207-2016, 2016.

Diao, X., Zhang, Y., and Chen, K. Z.: The global recession and China's stimulus package: A general equilibrium assessment of country level impacts, China. Econ. Rev., 23, 1-17, doi: 10.1016/j.chieco.2011.05.005, 2012.

Dou, L.: A research on the impact of industrialization on the environment in Xinjiang with an empirical analysis, Mater thesis, Xinjiang University, Urumqi, 2009 (in Chinese).

Fathian, F., Dehghan, Z., Bazrkar, M. H., and Eslamian, S.: Trends in hydrological and climatic variables affected by four variations of the Mann-Kendall approach in Urmia Lake Basin, Iran. Hydrolog. Sci. J., 61, 892-904, doi: 10.1080/02626667.2014.932911, 2016.

Fioletov, V. E., McLinden, C. A., Krotkov, N., and Li, C.: Lifetimes and emissions of SO_2 from point sources estimated from OMI, Geophys. Res. Lett., 42, 1969-1976, doi: 10.1002/2015GL063148, 2015.

Fioletov, V. E., McLinden, C. A., Krotkov, N., Li, C., Joiner, J., Theys, N., Carn, S., and Moran, M. D.: A global catalogue of large SO_2 sources and emissions derived from the Ozone Monitoring Instrument, Atmos. Chem. Phys., 16, 11497–11519,

doi: 10.5194/acp-16-11497-2016, 2016.
Gao, T., and Shi, X.: Spatio-temporal characteristics of extreme precipitation events during 1951-2011 in Shandong, China and possible connection to the large scale atmospheric circulation, Stoch. Env. Res. Risk. A., 30, 1421-1440, doi: 10.1007/s00477-015-1149-7, 2016.
Han, Y.; Gao, J.; Li, H; and Li, Y.: Ecological suitability analysis on the industry overall arrangement plan of Ningdong energy sources and chemical industry base, Environ. Sci. Manager, 32, 142-147,2007 (in Chinese).
He, D., Zhang, Z., and Zhang, W.: How large will be the effect of China's fiscal stimulus package on output and employment, Pacific Economic Review, 14, 730-744, doi: 10.1111/j.1468-0106.2009.00480.x, 2009.
Huang, T., Jiang, W., Ling, Z., Zhao, Y., Gao, H., and Ma, J.: Trend of cancer risk of Chinese inhabitants to dioxins due to changes in dietary patterns 1980-2009, Sci. Rep., 6, doi: 10.1038/srep21997, 2016.
Ialongo, I., Hakkarainen, J., Kivi, R., Anttila, P., Krotkov, N. A.,Yang, K., Li, C., Tukiainen, S., Hassinen, S., and Tamminen, J.: Comparison of operational satellite SO_2 products with ground-based observations in northern Finland during the Icelandic Holuhraun fissure eruption, Atmos. Meas. Tech., 8, 2279-2289, doi: 10.5194/amt-8-2279-2015, 2015.
Jiang, J., Zha, Y., Gao, J., and Jiang, J.: Monitoring of SO_2 column concentration change over China from Aura OMI data, Int. J. Remote Sen., 33, 1934-1942, doi: 10.1080/01431161.2011.603380, 2012.

Kanada, M., Dong, L., Fujita, T., Fujita, M., Inoue, T., Hirano, Y., Togawa, T., and Geng, Y.: Regional disparity and cost-effective SO_2 pollution control in China: A case study in 5 mega-cities, Energ. Policy, 61, 1322-1331, doi:10.1016/j.enpol.2013.05.105, 2013.

Kendall, M. G., and Charles, G.: Rank correlation methods, Oxford Univ. Press, New York., USA, 202 pp., 1975.

Krotkov, N. A., Carn, S. A., Krueger, A. J., Bhartia, P. K., and Yang, K.: Band Residual Difference Algorithm for Retrieval of SO_2 From the Aura Ozone Monitoring Instrument (OMI), IEEE T. Geosci. Remote, 44, 1259-1266, doi:10.1109/TGRS.2005.861932, 2006.

Krotkov, N. A., McClure, B., Dickerson, R. R., Carn, S. A., Li, C., Bhartia, P. K., Yang, K., Krueger, A. J., Li, Z., Levelt, P. F., Chen, H., Wang, P., and Lu, D.: Validation of SO_2 retrievals from the Ozone Monitoring Instrument over NE China, J. Geophys. Res., 113, D16S40, doi:10.1029/2007JD008818, 2008.

Krotkov, N. A., McLinden, C. A., Li, C., Lamsal, L. N., Celarier, E. A., Marchenko, S. V., Swartz, W. H., Bucsela, E. J., Joiner, J., Duncan, B. N., Boersma, K. F., Veefkind, J. P., Levelt, P. F., Fioletov, V. E., Dickerson, R. R., He, H., Lu, Z., and Streets, D. G.: Aura OMI observations of regional SO_2 and NO_2 pollution changes from 2005 to 2015, Atmos. Chem. Phys., 16, 4605-4629, doi: 10.5194/acp-16-4605-2016, 2016.

Kurokawa, J., Ohara, T., Morikawa, T., Hanayama, S., Greet, J. M., G., Fukui, T., Kawashima, K., and Akimoto, H.: Emissions of air pollutants and greenhouse gases over Asian regions during 2000–2008: Regional Emission Inventory in Asia (REAS) version 2, Atmos. Chem. Phys., 13, 11019–11058, doi: 10.5194/acp-13-11019-2013, 2013.

Levelt, P. F., Van der Oord, G. H. J., Dobber, M. R., Malkkl, A., Visser, H., De Vries, J., Stammes, P., Lundell, J., Saari, H.: The ozone monitoring instrument. IEEE Transactions on Geoscience and Remote Sensing, 44, 1093-1101, doi:10.1109/TGRS.2006.872333, 2006a.

Levelt, P. F., Hilsenrath, E., Leppelmeier, G. W., Oord, G. H. J. Van Den, Bhartia, P. K., Tamminen, J., De Haan, J. F., and Veefkind, J. P.: Science Objectives of the Ozone Monitoring Instrument, IEEE T. Geosci. Remote Sens., 44, 1199-1208, 2006b.

Li, C., Joiner, J., Krotkov, N. A., and Bhartia, P. K.: A fast and sensitive new satellite SO_2 retrieval algorithm based on principal component analysis: Application to the Ozone Monitoring Instrument, Geophys. Res. Lett., 40, 6314-6318, doi: 10.1002/2013GL058134,2013.

Li, C., Wang, R., Ning, H., and Luo, Q.: Changes in climate extremes and their impact on wheat yield in Tianshan Mountains region, northwest China, Environ. Earth Sci., 75, doi: 10.1007/s12665-016-6030-6, 2016.

Li, C., Zhang, Q., Krotkov, N. A., Streets, D. G., He, K., Tsay, S. C., and Gleason, J. F.: Recent large reduction in sulfur dioxide emissions from Chinese power plants observed by the Ozone Monitoring Instrument, Geophys. Res. Lett., 37, L08807, doi: 10.1029/2010GL042594, 2010.

Li, M., Zhang, Q., Kurokawa, J., Woo, J., He, K., Lu, Z., Ohara, T., Song, Y., Streets, D. G., Carmichael, G. R., Cheng, Y., Hong, C., Huo, H., Jiang, X., Kang, S., Liu, F., Su, H., and Zheng, B.: MIX: a mosaic Asian anthropogenic emission inventory under the international collaboration framework of the MICS-Asia and HTAP, Atmos. Chem. Phys., 17, 935-963, doi: 10.5194/acp-17-935-2017, 2017.

Lu, Z., Streets, D. G., Zhang, Q., Wang, S., Carmichael, G. R., Cheng, Y. F., Wei, C., Chin, M., Diehl, T., and Tan, Q.: Sulfur dioxide emissions in China and sulfur trends in East Asia since 2000, Atmos. Chem. Phys., 10, 6311-6331, doi: 10.5194/acp-10-6311-2010, 2010.

Lu, Z., Zhang, Q., and Streets, D. G.: Sulfur dioxide and primary carbonaceous aerosol emissions in China and India, 1996-2010, Atmos. Chem. Phys., 11, 9839-9864,doi: 10.5194/acp-11-9839-2011, 2011.

Ma, J., and Xu, J.: China's energy rush harming ecosystem, Nature, 541-30, doi: 10.1038/541030b, 2017.

Mann, H. B.: Nonparametric tests against trend, Econometrica, 13, 245-259, doi: 10.2307/1907187, 1945.

McLinden, C. A., Fioletov, V., Boersma, K. F., Kharol, S. K., Krotkov, N., Lamsal, L., Makar, P. A., Martin, R. V., Veefkind, J. P., and Yang, K.: Improved satellite retrievals of NO_2 and SO_2 over the Canadian oil sands and comparisons with surface measurements, Atmos. Chem. Phys., 14, 3637–3656, doi:10.5194/acp-14-3637-2014, 2014.

McLinden, C. A., Fioletov, V., Krotkov, N. A., Li, C., Boersma, K. F., and Adams, C.:

A decade of change in NO_2 and SO_2 over the Canadian oil sands as seen from space, Environ. Sci. Technol., 50, 331-337, doi: 10.1021/acs.est.5b04985, 2015.

McLinden, C. A., Fioletov, V., Shephard, M. W., Krotkov, N., Li, C., Martin, R. V., Moran, M. D., and Joiner, J.: Space-based detection of missing sulfur dioxide sources of global air pollution, Nature Geosci., 9, 496-500, doi: 10.1038/ngeo2724, 2016.

MEPC (Ministry of Environmental Protection of China): Ambient air quality standards, Available at: http://kjs.mep.gov.cn/hjbhbz/bzwb/dqhjbh/dqhjzlbz/201203/t20120302_224165.shtml (last access:21 January 2017), 2012 (in Chinese).

Moraes, J. M., Pellegrino, G. Q., Ballester, M. V., Martinelli, L. A., Victoria, R. L., and Krusche, A. V.: Trends in hydrological parameters of a southern Brazilian watershed and its relation to human induced changes, Water Resour. Manag., 12, 295-311, doi: 10.1023/A:1008048212420, 1998.

NBSC(National Bureau of Statistics of China): China Energy Statistical Yearbook 2005, China Statistics Press, Beijing, 2005.

NBSC(National Bureau of Statistics of China): China Energy Statistical Yearbook 2006, China Statistics Press, Beijing, 2006.

NBSC(National Bureau of Statistics of China): China Energy Statistical Yearbook 2011, China Statistics Press, Beijing, 2011.

NBSC(National Bureau of Statistics of China): China Energy Statistical Yearbook 2015, China Statistics Press, Beijing, 2015.

Ohara, T., Akimoto, H., Kurokawa, J., Horii, N., Yamaji, K., Yan, X., and Hayasaka, T.: An Asian emission inventory of anthropogenic emission sources for the period 1980–2020, Atmos. Chem. Phys., 7, 4419-4444, doi: 10.5194/acp-7-4419-2007, 2007.

Sharma, C. S., Panda, S. N., Pradhan, R. P., Singh, A., and Kawamura, A.: Precipitation and temperature changes in eastern India by multiple trend detection methods, Atmos. Res., 180, 211-225, doi: 10.1016/j.atmosres.2016.04.019, 2016.

Shen, Y., Zhang, X., Brook, J. R., Huang, T., Zhao, Y., Gao, H., and Ma, J.: Satellite remote sensing of air quality in the Energy Golden Triangle in Northwest China, Environ. Sci. Technol. Lett., 3,275-279, doi: 10.1021/acs.estlett.6b00182, 2016.

Sicard, P., Serra, R., and Rossello, P.: Spatiotemporal trends in ground-level ozone concentrations and metrics in France over the time period 1999-2012, Environ. Res., 149, 122-144, doi:10.1016/j.envres.2016.05.014, 2016.

Smith, S. J., van Aardenne, J., Klimont, Z., Andres, R. J.,Volke, A., and Delgado Arias, S.: Anthropogenic sulfur dioxide emissions: 1850-2005, Atmos. Chem. Phys., 11, 1101-1116,doi:10.5194/acp-11-1101-2011, 2011.

Stevenson, D. S., Johnson, C. E., Collins, W. J., and Derwent,R. G.: The atmospheric sulphur cycle and the role of volcanic SO_2, Geol. Soc. Lond. Spec. Publ., 213, 295-305, doi: 10.1144/GSL.SP.2003.213.01.18, 2003.

Su, S., Li, B., Cui, S., and Tao, S.: Sulfur Dioxide Emissions from Combustion in China: From 1990 to 2007, Environ. Sci. Technol., 45, 8403-8410, doi:

10.1021/es201656f, 2011.

Waked, A., Sauvage, S., Borbon, A., Gauduin, J., Pallares, C., Vagnot, M. P., Thierry, L., and Locoge, N.: Multi-year levels and trends of non-methane hydrocarbon concentrations observed in ambient air in France, Atmos. Environ., 141, 263-275, doi: 10.1016/j.atmosenv.2016.06.059, 2016.

Wang, S., Zhang, Q., Martin, R.V., Philip, S., Liu, F., Li, M., Jiang, X., and He, K.: Satellite measurements oversee China's sulfur dioxide emission reductions from coal-fired power plants, Environ. Res. Lett., 10, 114015, doi: 10.1088/1748-9326/10/11/114015, 2015.

Wang, S., Satellite remote sensing of the sulfur dioxide and nitrogen dioxide emissions from coal-fired power plants, PhD thesis, Tsinghua University, Beijing, 2014.

Wang, Z., Shao, M., Chen, L., Tao, M., Zhong, L., Chen, D., Fan, M., Wang, Y., and Wang, X.: Space view of the decadal variation for typical air pollutants in the Pearl River Delta (PRD) region in China, Front. Env. Sci. Eng., 10, doi: 10.1007/s11783-016-0853-y, 2016.

Whelpdale, D. M., Dorling, S. R., Hicks, B. B., and Summers, P.W.: Atmospheric process in: Global Acid Deposition Assessment, edited by: Whelpdale, D. M., and Kaiser, M. S., World Meteorological Organization Global Atmosphere Watch, Report Number 106, Geneva, 7-32, 1996.

Yan, H., Chen, L., Su, L., Tao, J., and Yu, C.: SO_2 columns over China: Temporal and spatial variations using OMI and GOME-2 observations, 35th International

Symposium on Remote Sensing of Environment, 17, 012027, doi: 10.1088/1755-1315/17/1/012027, 2014.

Yue, S and Pilon, P.: A comparison of the power of the t-test, Mann-Kendall and bootstrap tests for trend detection, Hydrolog. Sci. J., 49, 21-37, doi: 10.1623/hysj.49.1.21.53996, 2004.

Yue, S., and Wang, C.: The Mann-Kendall test modified by effective sample size to detect trend in serially correlated hydrological series, Water Resour. Manag., 18, 201-218, doi: 10.1023/B:WARM.0000043140.61082.60, 2004.

Zhang, X., Huang, T., Zhang, L., Gao, H., Shen, Y., and Ma, J.: Trends of deposition fluxes and loadings of sulfur dioxide and nitrogen oxides in the artificial Three Northern Regions Shelter Forest across northern China, Environ. Pollut., 207, doi: 10.1016/j.envpol.2015.09.022 238-247, 2015.

Zhang, X., Huang, T. Zhang, L., Shen, Y., Zhao, Y., Gao, H., Mao, X., Jia, C., and Ma, J.: Three-North Shelter Forest Program contribution to long-term increasing trends of biogenic isoprene emissions in northern China, Atmos. Chem. Phys., 16, 6949-6960, doi: 10.5194/acp-16-6949-2016, 2016.

Zhang, Y., Guan, D., Jin, C., Wang, A., Wu, J., and Yuan, F.: Analysis of impacts of climate variability and human activity on stream flow for a river basin in northeast China, J. Hydrol., 410, 239-247, doi: 10.1016/j.jhydrol.2011.09.023, 2011.

Zhao, B., Wang, S. X., Liu, H., Xu, J. Y., Fu, K., Klimont, Z., Hao,J. M., He, K. B., Cofala, J., and Amann, M.: NOx emissions in China: historical trends and future perspectives, Atmos. Chem. Phys., 13, 9869–9897, doi: 10.5194/acp-13-9869-2013, 2013.

Zhao, H., Li, X., Zhang, Q., Jiang, X., Lin, J., Peters, G. G., Li, M., Geng, G., Zheng, B., Huo, H., Zhang, L., Davis, S. J., and He, K.: Effects of atmospheric transport and trade on air pollution mortality in China, Atmos. Chem. Phys. Discuss., doi:10.5194/acp-2017-263, in review, 2017.

Zhao, L.: Strategic thinking on construction of Ningdong Energy Chemical Base and development of Ningxia Coal Industry Group, Northwest Coal, 4, 11-13, 2016 (in Chinese).

Zhao, Y., Huang, T., Wang, L., Gao, H., and Ma, J.: Step changes in persistent organic pollutants over the Arctic and their implications, Atmos. Chem. Phys., 15, 3479-3495, doi: 10.5194/acp-15-3479-2015, 2015.

Zhao, Y., Nielsen, C. P., Lei, Y., McElroy, M. B., and Hao, J.: Quantifying the uncertainties of a bottom-up emission inventory of anthropogenic atmospheric pollutants in China, Atmos. Chem. Phys., 11, 2295–2308, doi: 10.5194/acp-11-2295-2011, 2011.

Zhu, J.; and Ruth, M.: Relocation or reallocation: Impacts of differentiated energy saving regulation on manufacturing industries in China, Ecol. Econ., 110, 119−133, doi: 10.1016/j.ecolecon.2014.12.020, 2015.

Table 1 Annual growth rate for OMI SO_2 VCD and economic activities for individual provinces and municipality during 2005-2014 (% yr^{-1}), and SO_2 emission reduction plan during the 11th and 12th Five-Year Plan period (%).

Region		OMI SO_2 VCD	coal consumption	Industrial GDP	Thermal power generation	steel production	SO_2 emission reduction plan (%)	
							2006-2010[a]	2011-2015[b]
Northwestern	Inner Mongolia	0.94	11.29	20.48	14.07	8.38	-3.8	-3.8
	Shaanxi	-3.41	13.14	19.96	13.01	14.48	-12	-7.9
	Gansu	-0.09	6.69	14.19	8.89	9.92	0	2.0
	Qinghai	0.69	11.20	18.70	9.88	12.37	0	16.7
	Ningxia	0.95	11.79	17.44	15.04	152.71	-9.3	-3.6
	Xinjiang	1.57	17.21	14.21	23.39	16.27	0	0
BTH	Beijing	-3.59	-6.13	9.13	5.99	-48.52	-20.4	-13.4
	Tianjin	-4.63	3.15	15.84	6.01	10.19	-9.4	-9.4
	Hebei	-5.05	4.16	12.37	6.22	10.70	-15	-12.7
YRD	Shanghai	-7.65	-0.93	6.64	0.86	-0.92	-26.9	-13.7
	Jiangsu	-5.93	5.39	12.51	7.49	13.35	-18.0	-14.8
	Zhejiang	-2.07	4.04	11.40	8.68	13.94	-15.0	-13.3
PRD	Guangdong	-4.55	6.15	12.03	5.92	6.87	-15.0	-14.8

a and b represents proposed reduction in SO_2 emission in 2010 relative to 2005, and 2015 relative to 2010, respectively. The value for PRD refers to the proposed target for Guangdong Province.

Figure Captions

Figure 1 Selected regions in this investigation across China, including Northwestern China, defined by pink slash, includes Inner Mongolia, Shaanxi, Gansu, Qinghai, Ningxia, Beijing-Tianjin-Hebei (BTH), the North China Plain (NCP), the Sichuan Basin, Yangtze River Delta (YRD), and Pearl River Delta (PRD). These regions are labeled in the figure and marked by different colors as shown in the figure. The Urumqi-Midong region (brick red color) and the Energy Golden Triangle (EGT, purple color) are also labeled in the figure. Red triangles indicate 188 monitoring sites across China. Blue circles indicate 6 selected cities in **Fig. 2**.

Figure 2 Annually averaged SO_2 VCD (DU), scaled on the right-hand-side y-axis and measured annual SO_2 air concentration (μg/m^3), scaled on the left-hand-side y-axis, in Beijing, Shanghai, Chongqing, Guangzhou, Yinchuan, and Urumqi.

Figure 3 Annually averaged SO_2 VCD (DU), scaled on the right-hand-side y-axis and annual emissions (thousand ton/yr) of SO_2 on the left-hand-side y-axis in the NCP, YRD, PRD, Sichuan Basin, EGT, and Urumqi-Midong region.

Figure 4 Annual averaging OMI-retrieved vertical column densities of SO_2 (DU) and their trends from 2005 to 2015 on $0.25^{\circ} \times 0.25^{\circ}$ latitude/longitude resolution in China. (**a**). Annual mean SO_2 vertical column densities; (**b**). slope (trend) of linear regression relationship between annual averaging OMI-retrieved SO_2 VCD and the time sequence from 2005 to 2015 over China. The positive values indicate an increasing trend of SO_2 VCD from 2005 to 2015, and vice versa. The blue circle highlights the six selected regions including NCP (a), YRD (b), PRD (c), Sichuan Basin (d), Energy Golden Triangle (EGT, e), and Urumqi-Midong region (f).

Figure 5 Percentage changes in annual mean OMI SO_2 VCD relative to 2005 in four highlighted regions in eastern and southern China and two large-scale energy industry bases in the EGT and Urumqi-Midong region in **Figure 4b**.

Figure 6 Mann-Kendall (MK) test statistics for annually SO_2 VCD in those highlighted regions (**Figs. 1** and **4b)** from 2005-2015. The blue solid line is the forward sequence UF_k and the red solid line is the backward sequence UB_k defined by Eq (5). The positive values for UF_k indicate an increasing trend of SO_2 VCD, and vice versa. Two straight solid lines stand for confidence interval between -1.96 (straight green line) and 1.96 (straight purple line) in the MK test. The intersection of UF_k and UB_k sequences within the intervals between two confidence levels indicates a step change point.

Figure 7 Annual fractions of OMI retrieved SO_2 VCD and emissions averaged over 6 northwestern provinces in the national total SO_2 VCD from 2005 to 2015 and emission from 2005 to 2014. (**a**) fraction of annual mean SO_2 VCD; (**b**) fraction of annual mean emission. Fractions of SO_2 VCD are calculated as the ratio of the sum of annually averaged SO_2 VCD in northwestern China to the sum of annually averaged SO_2 VCD in the national total from 2005 to 2015 (%).

Figure 8 Per capita SO_2 emission in six provinces of northwestern China and three key eastern regions (tons/person). The value for PRD refers to the per capita SO_2 emission for Guangdong province.

Figure 9 Same as Fig. 6 but for Mann-Kendall (MK) test statistics for annually averaged SO_2 VCD in six provinces in northwestern China from 2005-2015.

Figure 10 Annually averaging OMI-retrieved vertical column densities of SO_2 (DU) in two major point sources, the MEIB in Xinjiang (a), and the NECIB in Ningxia (b).

Figure 11 Annually averaged SO_2 emissions (kt yr^{-1}) and SO_2 VCD (DU) in the NECIB and MEIB, and their fractions in provincial total SO_2 emission and ratios between SO_2 VCD in these two regions and that in province. (**a**). SO_2 emission (blue bar) in the NECIB and its fraction (red solid line) in the total provincial SO_2 emission in Ningxia. The left y-axis stands for SO_2 emission and the right y-axis denotes the fraction (%) at the upper panel and the error bars denotes the standard deviations of Source Detection Algorithm estimated SO_2 emission point sources; (**b**). same as Fig. 11a but for the MEIB. (**c**). SO_2 VCD (blue bar) in the NECIB and the ratio (red solid line) between SO_2 VCD in the NECIB and that in Ningxia. The left y-axis stands for SO_2 VCD (DU) and the right y-axis denotes the ratio at the lower panel; (**d**). same as Fig. 11c but for the MEIB.

Figure 1

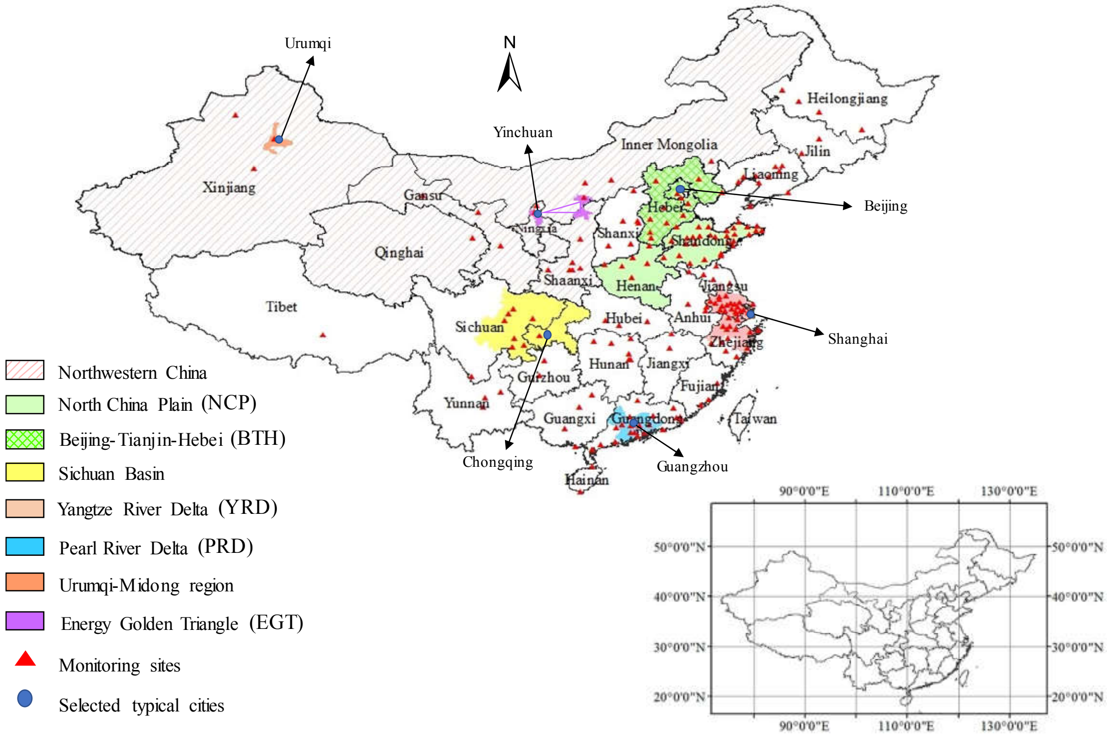
N
Urumqi
Yinchuan
Beijing
Shanghai
Chongqing
Guangzhou
Xinjiang
Tibet
Qinghai
Gansu
Ningxia
Inner Mongolia
Heilongjiang
Jilin
Liaoning
Hebei
Shanxi
Shandong
Shaanxi
Henan
Jiangsu
Anhui
Hubei
Sichuan
Zhejiang
Hunan
Jiangxi
Guizhou
Fujian
Yunnan
Guangxi
Guangdong
Taiwan
Hainan
Northwestern China
North China Plain (NCP)
Beijing-Tianjin-Hebei (BTH)
Sichuan Basin
Yangtze River Delta (YRD)
Pearl River Delta (PRD)
Urumqi-Midong region
Energy Golden Triangle (EGT)
Monitoring sites
Selected typical cities
90°0'0"E
110°0'0"E
130°0'0"E
50°0'0"N
40°0'0"N
30°0'0"N
20°0'0"N

Figure 2

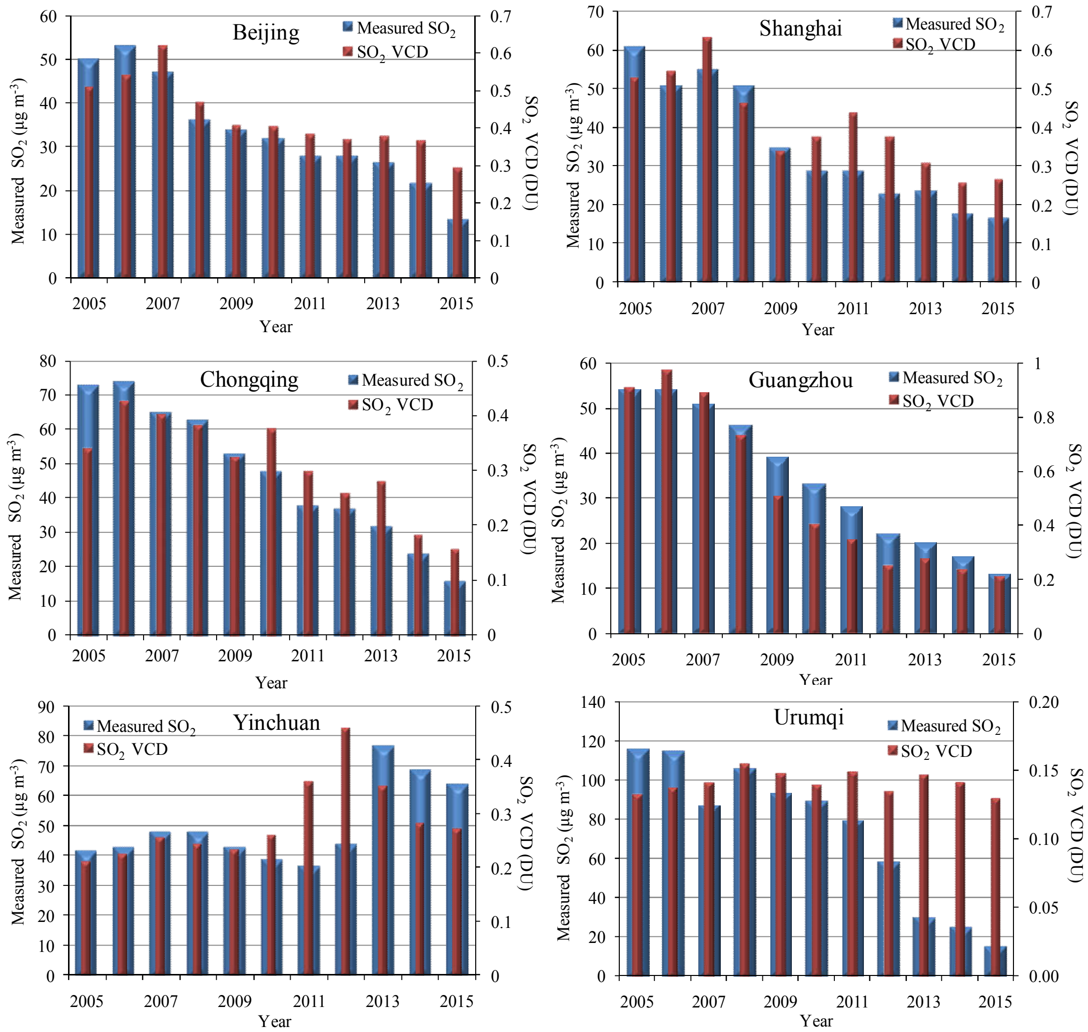
Beijing
Shanghai
Chongqing
Guangzhou
Yinchuan
Urumqi
Measured SO_2
SO_2 VCD
Measured SO_2 (μg m^{-3})
SO_2 VCD (DU)
Year
2005
2007
2009
2011
2013
2015

Figure 3

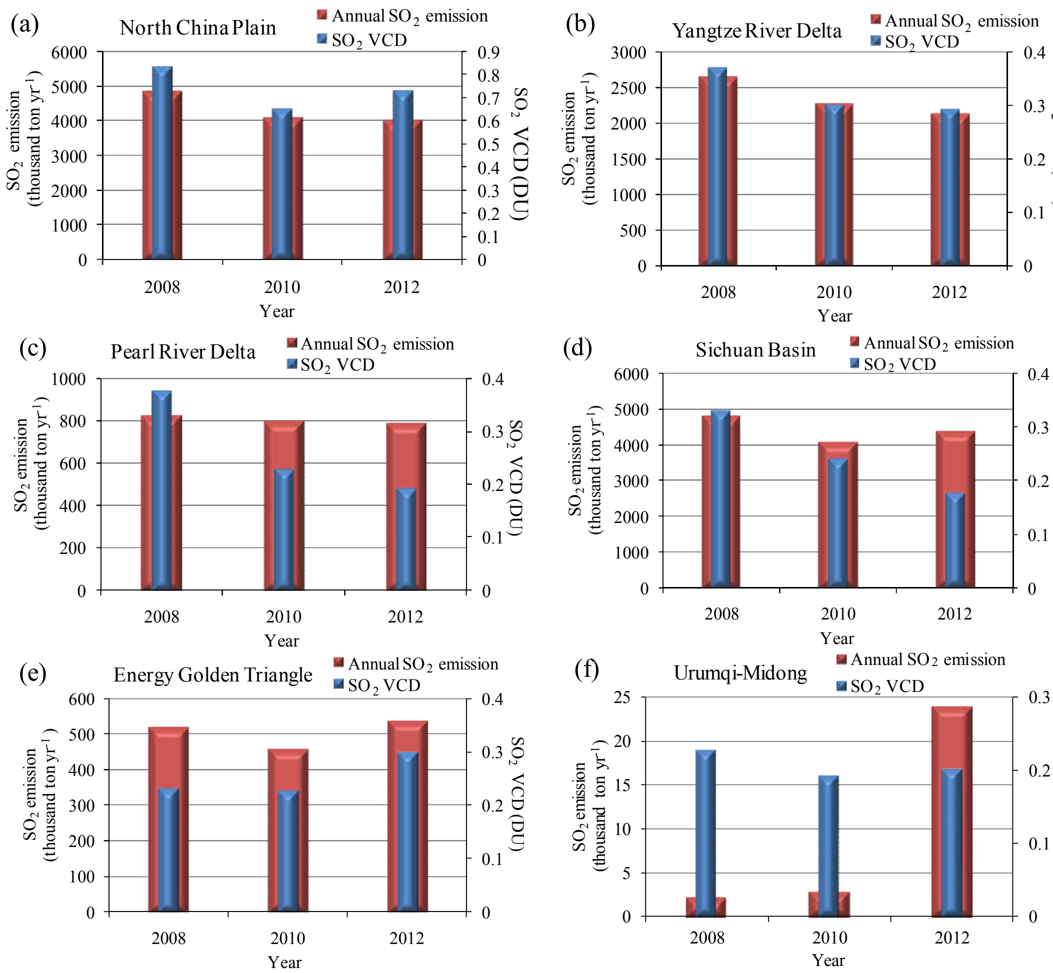

(a)
North China Plain
Annual SO_2 emission
SO_2 VCD
SO_2 emission (thousand ton yr^{-1})
SO_2 VCD (DU)
Year
(b)
Yangtze River Delta
Annual SO_2 emission
SO_2 VCD
SO_2 emission (thousand ton yr^{-1})
SO_2 VCD (DU)
Year
(c)
Pearl River Delta
Annual SO_2 emission
SO_2 VCD
SO_2 emission (thousand ton yr^{-1})
SO_2 VCD (DU)
Year
(d)
Sichuan Basin
Annual SO_2 emission
SO_2 VCD
SO_2 emission (thousand ton yr^{-1})
SO_2 VCD (DU)
Year
(e)
Energy Golden Triangle
Annual SO_2 emission
SO_2 VCD
SO_2 emission (thousand ton yr^{-1})
SO_2 VCD (DU)
Year
(f)
Urumqi-Midong
Annual SO_2 emission
SO_2 VCD
SO_2 emission (thousand ton yr^{-1})
SO_2 VCD (DU)
Year

Figure 4

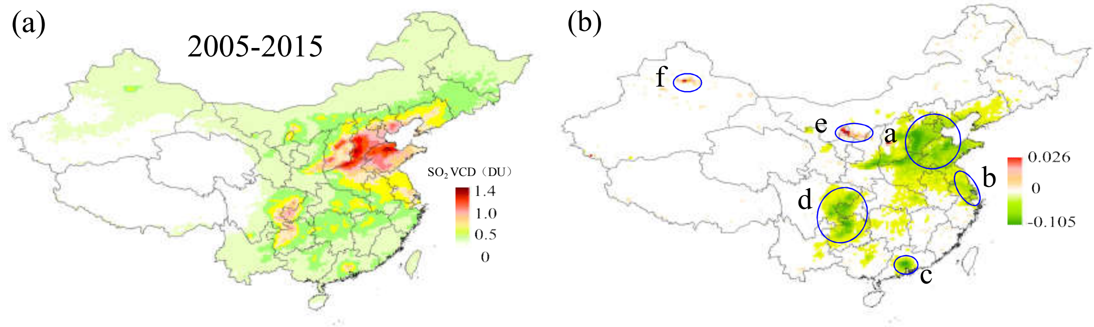

Figure 5

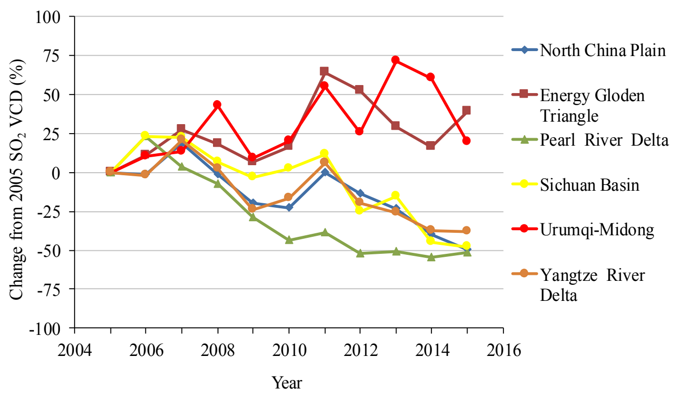

Figure 6

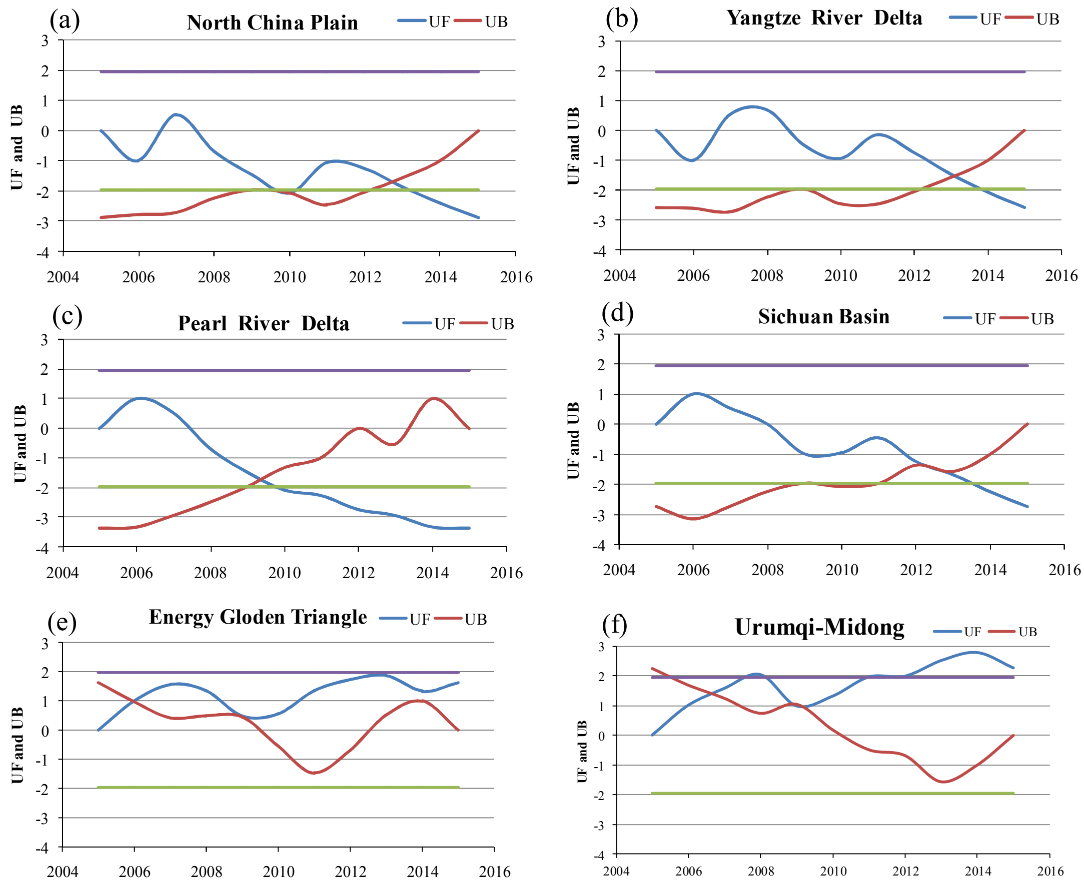

Figure 7

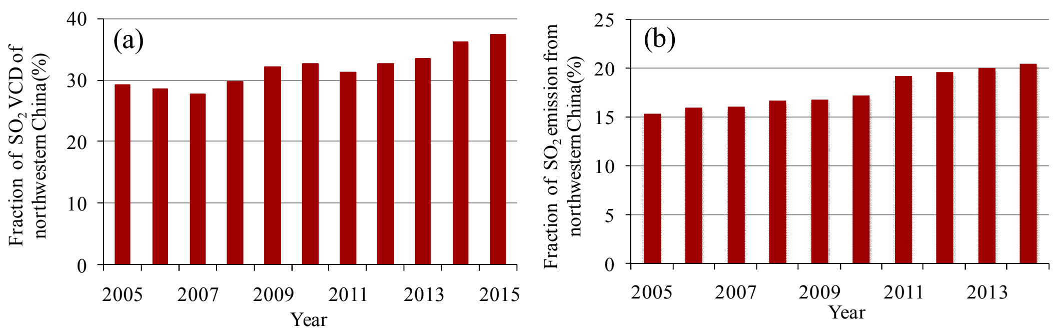

Figure 8

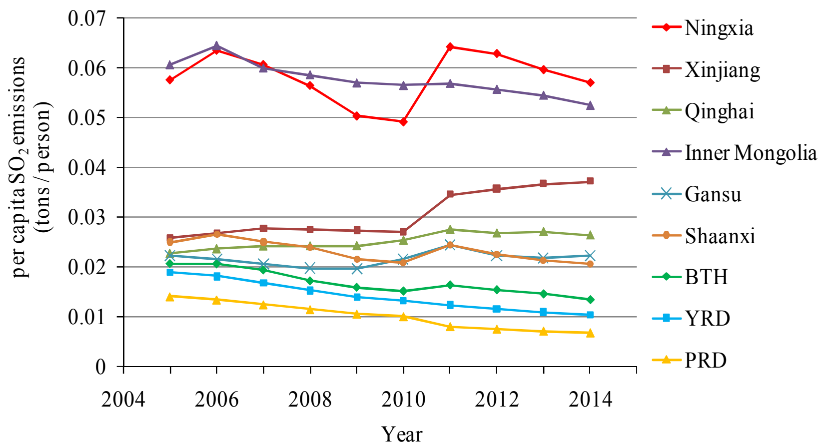

Figure 9

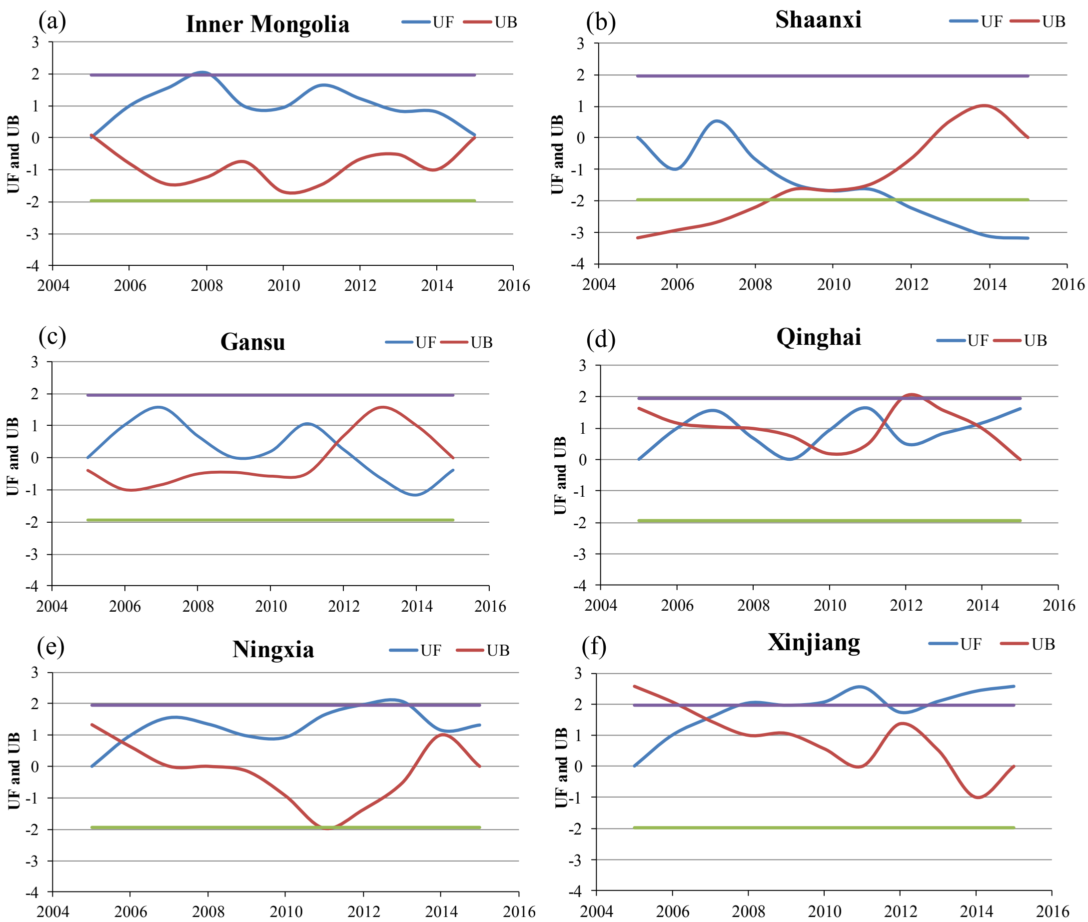

Figure 10

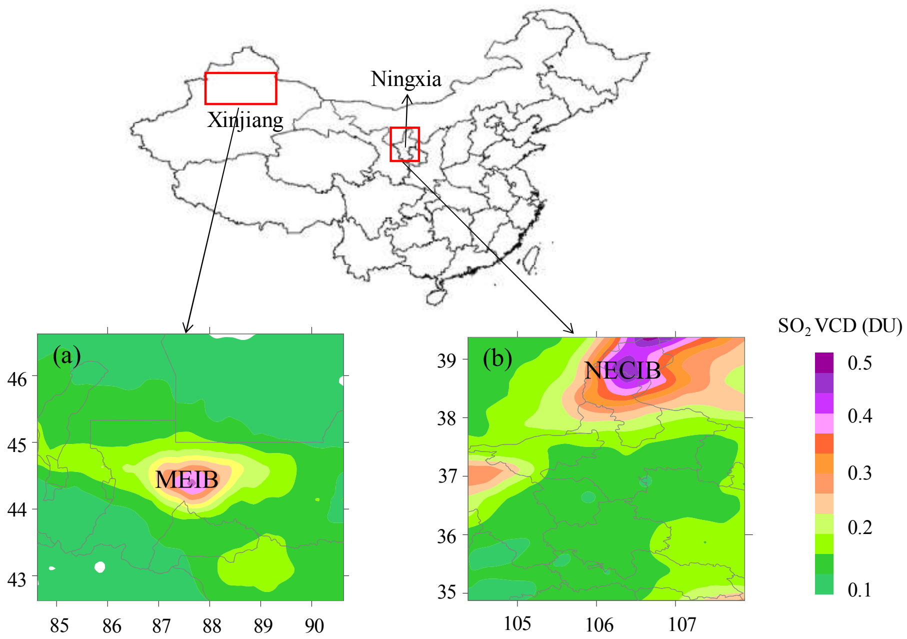

Figure 11